This is a repository copy of *Real Space Imaging of Nanoparticle Assembly at Liquid-Liquid Interfaces with Nanoscale Resolution.*.

White Rose Research Online URL for this paper:
http://eprints.whiterose.ac.uk/104641/

Version: Accepted Version

Real space imaging of nanoparticle assembly at liquid-liquid interfaces with nanoscale resolution

Luca Costa[1,2‡*], Giovanni Li-Destri[1‡*], Neil H. Thomson[3], Oleg Konovalov[1], Diego Pontoni[1]

[1] ESRF-The European Synchrotron 71, Avenue des Martyrs. 38100 Grenoble, France

[2] CBS, Centre de Biochimie Structurale, CNRS UMR 5048-INSERM UMR 1054, 29, Rue de Navacelles, 34090 Montpellier, France

[3] Department of Oral Biology, School of Dentistry and Molecular and Nanoscale Physics Group, School of Physics and Astronomy, University of Leeds, LS29JT Leeds, United Kingdom.

Bottom up self-assembly of functional materials at liquid-liquid interfaces has recently emerged as method to design and produce novel 2D nanostructured membranes and devices with tailored properties. Liquid-liquid interfaces can be seen as a "factory floor" for nanoparticle (NP) self-assembly, since NPs are driven there by a reduction of interfacial energy. Such 2D assembly can be characterised by reciprocal space techniques, namely X-ray and neutron scattering or reflectivity. These techniques have drawbacks however, as the structural information is averaged over the finite size of the radiation beam and non-periodic isolated assemblies in 3D or defects may not be easily detected. Real-space in-situ imaging methods are more appropriate in this context, but they often suffer from limited resolution and under-perform or fail when applied to challenging liquid-liquid interfaces. Here we study the surfactant-induced assembly of SiO_2 nanoparticle monolayers at a water-oil interface using in-situ atomic force microscopy (AFM) achieving nanoscale resolved imaging capabilities. Hitherto, AFM imaging has been restricted to solid-liquid interfaces since

1

applications to liquid interfaces have been hindered by their softness and intrinsic dynamics, requiring accurate sample preparation methods and non-conventional AFM operational schemes. Comparing both AFM and grazing incidence X-ray small angle scattering (GISAXS) data, we unambiguously demonstrate correlation between real and reciprocal space structure determination showing that the average interfacial NP density is found to vary with surfactant concentration. Additionally, the interaction between the tip and the interface can be exploited to locally determine the acting interfacial interactions. This work opens up the way to studying complex nanostructure formation and phase behaviour in a range of liquid-liquid and complex liquid interfaces.

KEYWORDS Nanomaterials, Thin films, Surface coverage, Force Spectroscopy, Inter-particle distance, Tapping Mode AFM.

Achieving high resolution imaging of liquid interfaces in the real space has always been challenging. Brewster Angle Microscopy (BAM) is widely employed but has a limited resolution. Other techniques such as super-resolved fluorescence microscopy can provide images[1] and even topographical information[2-3] with a resolution of few tens of nanometers but are limited to the localization of fluorescent molecules.

AFMs are excellent tools to characterize routinely solid/air[4-8] and solid/liquid[4,9-13] interfaces; the proper choice of experimental conditions has even allowed to image liquid-dispersed micrometer-sized drops and bubbles deposited on a solid substrate and to locally measure their interfacial tension[14]. However, despite very rare investigations limited to the liquid/air case[15-16], high resolution images of liquid interfaces containing morphological information have not yet been reported. Here we present an approach to perform routinely high resolution AFM imaging at liquid/liquid interfaces. We succeeded to characterize SiO_2 NP monolayers self-assembled at the water/heptane interface achieving a lateral resolution inferior to 10 nm. The main advantage of

these measurements is their very local nature which permits characterization of local defects such as holes and aggregates that cannot be detected easily by reciprocal space techniques.

Self-assembly of NP at liquid-liquid interfaces has recently raised considerable fundamental scientific interest[17] and demonstrates great potential for technological applications[18] based on the magnetic, electronic or optical[19] nature of the NP core. This represents an emerging strategy to obtain novel materials via massively parallel assembly of nanoscale building blocks characterized by extraordinary physical and chemical properties and allowing fabrication of complex hierarchical structures[20-22].

Reciprocal space techniques such as grazing incidence small angle X-Ray scattering (GISAXS) are widely employed to characterize these systems[23]. However, in order to get structural information on localized areas of the interface, real space imaging is required. This, so far, has been achieved only ex-situ, by transmission electron microscopy (TEM)[24-25] or for limited cases of interfaces containing fluorescent molecules[19]. Here we investigate the self-assembly of silica NPs onto the flat interface of a water sub-phase in contact with a bulk phase of immiscible oil, such as hexane or heptane. A cationic surfactant, namely cetyl trimethylammonium bromide (CTAB), dissolved in the water sub-phase in sub-millimolar concentrations, decorates the NPs to make them amphiphilic, thus they spontaneously adsorb at the interface[26-27]. Depending on the amount of adsorbed CTAB it is possible to control the monolayer density[27] and, as we will show below, the inter-particle distance. In this work we investigate two concentrations of CTAB at 0.01 mM and 0.05 mM, for monolayers of CTAB-decorated SiO_2 NPs ($\approx$ 20 nm diameter) adsorbed at the water/oil interface by AFM and GISAXS. AFM was employed to both characterize the interfacial forces and the morphology of the NP monolayers in real space in situ for the first time, showing full consistency with the reciprocal space GISAXS results.

We have employed Amplitude-Modulation mode AFM (AM-AFM)[28], which has been already exploited for the three-dimensional imaging of solid/liquid interfaces[29], to image two monolayers of CTAB-decorated SiO_2 nanoparticles (NPs) adsorbed at the water/hexane interface. In both cases,

the monolayer was left to equilibrate for half an hour under continuous hexane refilling, then hexane was slowly substituted with heptane which, owing to the lower surface pressure, evaporates more slowly and thus allows reproducible AFM imaging without continuous solvent refilling. The set-up is presented in Fig. 1a. A key point is the depth of the water layer, which has been kept below 100 μm to avoid surface waves originating in deeper water layers[30]. The cantilever is excited with a blue laser using a photothermal excitation operational scheme[31]. This set-up is capable to in-situ locally image the NP monolayers with unprecedented nanometric resolution, thus displaying not only the single particles but also local single nanoscopic defects (see Fig.1a inset) which cannot be detected by reciprocal space techniques. Fig. 1b reports AFM images of 0.01 mM CTAB-decorated 20 nm diameter NP monolayers where single NPs can be distinguished. Fig. 1d shows the AFM images for 0.05 mM CTAB-decorated NPs monolayers. We clearly observe higher interface coverage at higher CTAB concentration. This higher coverage is directly related to the reduced inter-particle distance (ID) which, at 0.05 mM CTAB concentration, does not allow the AFM tip to penetrate in between single NPs (Fig. 1e). As a consequence, NPs are observed to have a diameter close to 20 nm (Fig. 1e inset) consistent with that determined by small angle X-ray scattering (SAXS) data for NPs in solution (see Supporting Information Fig. 1). By contrast, at 0.01 mM CTAB concentration the ID is larger and the tip can penetrate in between single NPs (Fig. 1c). As a consequence, the convolution between the tip and the NPs produces AFM images with larger effective NP diameters (≈25nm) (Fig. 1c inset) compared to the 0.05 mM CTAB case. These images report the highest lateral resolution ever achieved by AFM at a liquid interface. Additional AFM images acquired with larger and smaller scan size are reported in the Supporting Information (Fig. S2). It must be noted that, due to the fluid nature of the interface, lateral drift of the samples, at speeds as high as fractions of μm/sec, may severely hamper the imaging (see Fig. S3). Therefore, fast imaging, typically an image acquisition time between 25 and 50 seconds, is required to minimize the drift effect on the image quality. Additionally, diffusion may severely hamper the

imaging in the case of sparse or inhomogeneous samples, thus dense homogeneous layers are currently preferred to perform reliable and reproducible imaging.

From these AFM images it is also possible to measure the NP interface coverage as $\Phi = N\,\pi\,R^2 / A$, where N is the number of NPs in a given area A and R the NP radius[32] (see Supporting Information 4 for a more detailed description of the surface coverage measurements). Since the NP radius value could be affected by tip convolution effect, we employed for the calculation the value determined by SAXS (see Fig. S1). As expected, the measured surface coverage increases with CTAB concentration, resulting in $\Phi_{0.05\ CTAB} = 0.53 \pm 0.06$ and $\Phi_{0.01\ CTAB} = 0.40 \pm 0.06$. In the assumption of hexagonally closed packed nanoparticles (see white hexagon in Fig. 1), the ID can be directly calculated from the surface coverage values as

$$ID = \sqrt{\frac{2\pi R^2}{\Phi\sqrt{3}}} = \sqrt{\frac{2A}{N\sqrt{3}}}$$

For the monolayer formed at CTAB 0.01 mM the inter-particle distance is 28.7 ± 2.7 nm, whereas for the one formed at CTAB 0.05 mM is 24.6 ± 2.5 nm. It should be noted that this NP counting approach, provided a known value of the NP radius, yields ID results that are not affected by the different apparent NP sizes observed at different CTAB concentrations. These values also explain why, despite only 4 nm difference between the two inter-particle distances, NPs at CTAB 0.01 mM are observed to be larger than the values extracted by SAXS. Indeed, at this condition, the wall-to-wall distance, that is the free available space between two adjacent NPs, is comparable to the tip radius (nominal value 8 nm), thus allowing the probe to penetrate between single nanoparticles (Fig. 1c) causing the above mentioned tip/NP convolution yielding a larger apparent NP diameter. This shows that the lateral and vertical resolution strongly depends on the AFM tip radius. An accurate calibration of both tip radius and tip-sample interaction force is required in order to extract quantitative topographical information of NPs monolayer if the NPs diameter or interfacial contact angle are unknown.
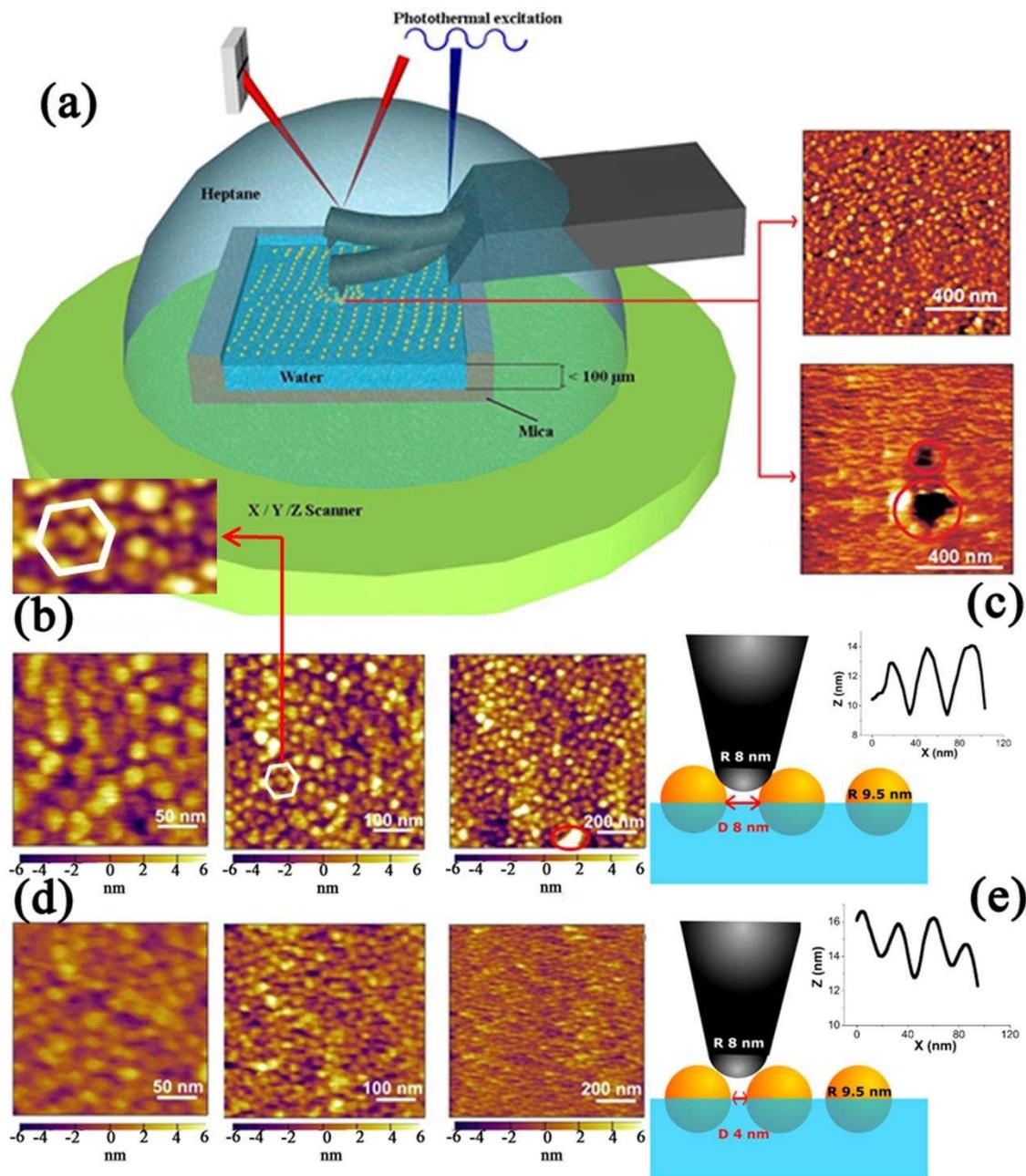
Figure 1: a AFM operational scheme and images of the NPs monolayers. The depth of the water layer confined by a mica container is kept inferior to 100 μm and the cantilever is excited by photothermal actuation (blue laser) inside the heptane drop. Inset: typical AFM images including ordered monolayers containing local defects such as holes and aggregates highlighted by red circles. **b-d** AFM images of the SiO_2 NP monolayers at the water/heptane interface as measured by AFM at different scan sizes, the white hexagon and the corresponding zoom highlights the local hexagonal packing of NPs. **b** Images of 0.01 mM (CTAB)-decorated SiO2 NP monolayers: since the wall-to-wall distance between adjacent NPs is comparable with the radius of curvature of the tip (**c**), the probe can penetrate between single nanoparticles and the tip/NP convolution yields a nanoparticle diameter slightly larger (≈ 25 nm) than the one determined by SAXS experiments, as evidenced by the morphological profile of the surface along three NPs in the inset. **d** Images of 0.05 mM (CTAB)-decorated SiO2 NPs monolayers: given a wall-to-wall distance inferior to the radius of curvature of the tip (**e**), the tip cannot penetrate between adjacent NPs.

The impact of the CTAB concentration on the inter-particle distance and interface coverage by NP is confirmed by GISAXS investigations performed on the same systems.

In Fig.2a-b GISAXS data from the two monolayers of CTAB-decorated SiO_2 nanoparticles (NPs) adsorbed at the water/hexane interface are reported. The inter-particle distance at the interface can be measured in situ by GISAXS[22,33]. Indeed, the two rods at +q_y and −q_y equidistant around q_y=0 are the structure factor peaks given by the interference of X-rays scattered by in plane correlated NPs and, in the assumption of hexagonally closed packed nanoparticles, their position (q_P) allows direct calculation of the inter-particle distance (ID) according to:

$$ID = \frac{4\pi}{\sqrt{3}q_p}$$

In Fig.2c-d the horizontal cuts of the GISAXS patterns together with their fits are reported. The ID is significantly higher for the monolayer formed at CTAB 0.01 mM (28.4±0.6 nm) than for the one formed at CTAB 0.05 mM (24.7±0.3 nm) and both values are fully consistent with the ones calculated from AFM images.
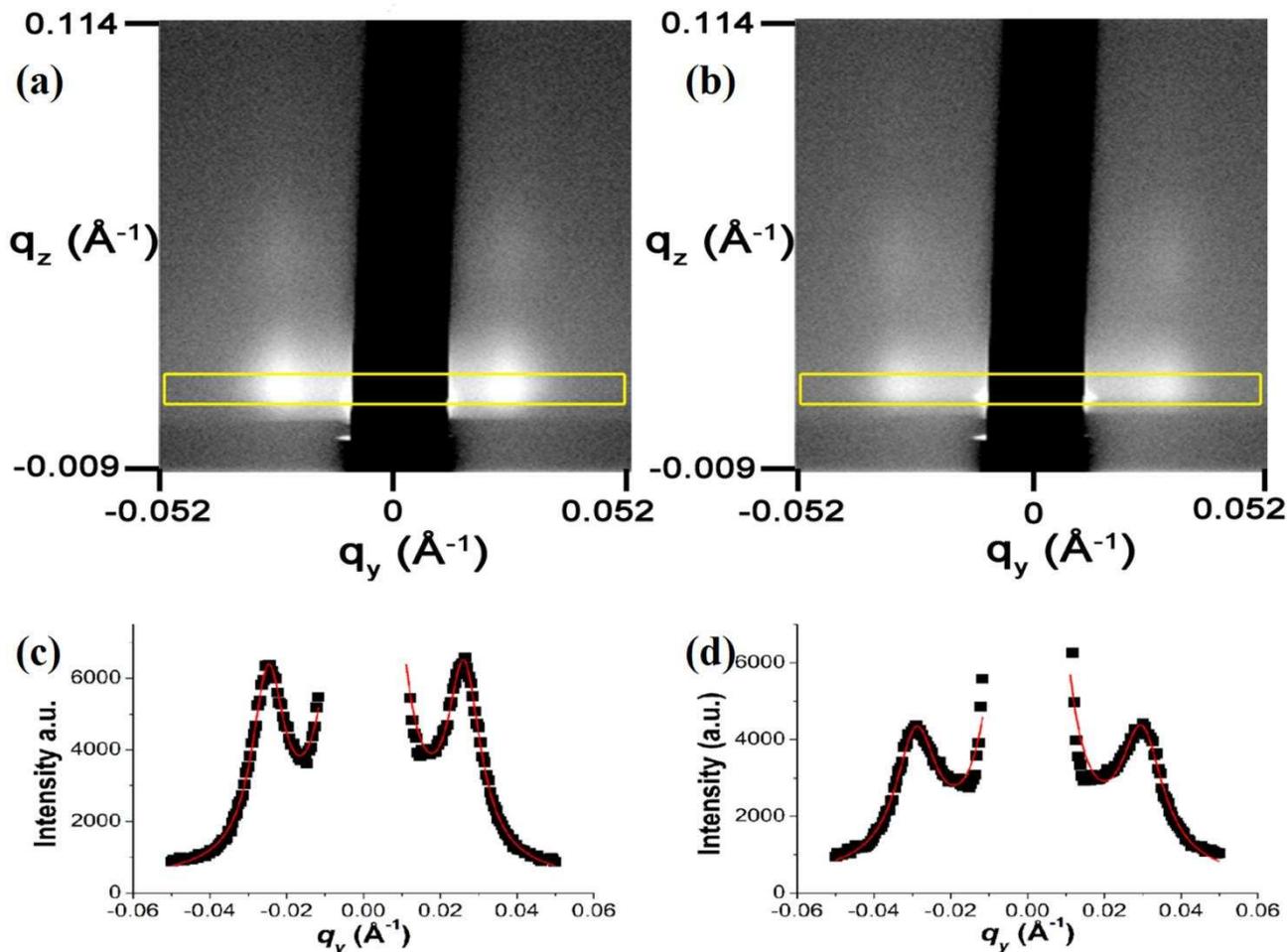
Figure 2: GISAXS 2D patterns of the NP monolayer at 0.01 mM CTAB (**a**) and 0.05 mM CTAB (**b**). Below each pattern is the corresponding horizontal cut at $0.024 < q_z < 0.026$ Å^{-1} (**c-d**), indicated by the yellow box in the 2D pattern, together with its best fit.

This proves that state of the art Atomic Force Microscopy is an excellent technique to investigate reliably in the real space, even at liquid-liquid interfaces having low interfacial stiffness. Complementary to reciprocal space investigations by neutron and X-Rays, AFM indeed provides very local images of the interface, including defects such as holes and aggregates (red circles in Fig. 1) that cannot be detected reliably by those techniques. Moreover, AFM can be employed to image rough 3D aggregates formed under higher CTAB concentrations (see Fig. S4), thus allowing to follow the progressive disruption of the 2D NP ordering.

In addition to nanoscale resolved imaging, AFM offers the possibility to characterize the interaction force between the tip and the interface. When approaching a non-oscillating AFM tip to the

liquid/liquid interface, we observe the absence of attractive forces (our force resolution is close to 100 pN). Once the mechanical contact between the tip and interface is established, the tip can indent the surface over several hundreds of nanometers[34,35], in contrast with the solid-liquid interface cases, as occurring when indenting complex fluid interfaces such living cells membranes[36-38]. Fig. 3 shows the Force vs Distance curves at the water/heptane interface in the absence (Blue) and presence (Red) of the 0.05mM CTAB NP monolayer.
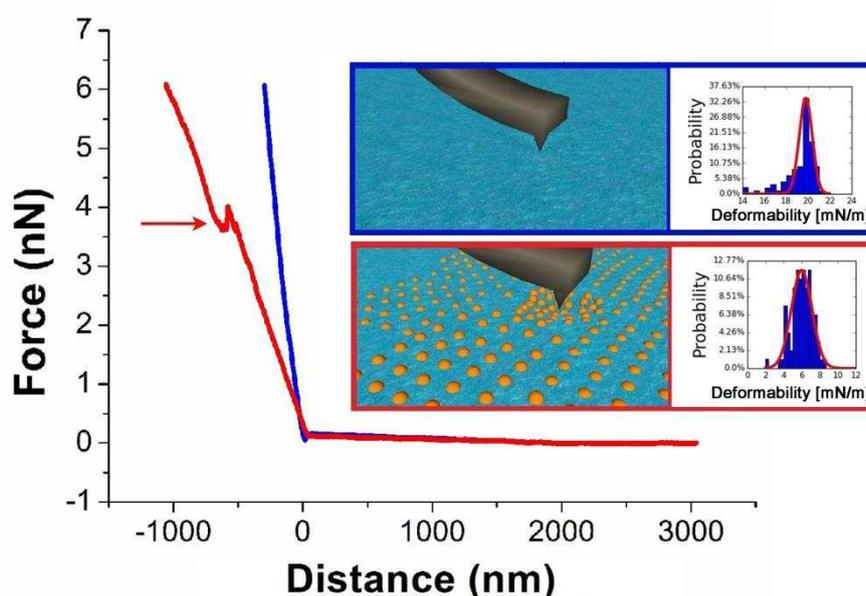
Figure 3: Indentation measurements at the water/heptane interface. **Blue** AFM Tip-interface interaction force as a function of their distance in the absence of the NP monolayer. **Red** AFM Tip-interface interaction force as a function of their reciprocal distance in presence of the 0.05 mM CTAB decorated NP monolayer: a discontinuity in the force curve is highlighted by the red arrow. **Inset:** Pictorial representation of the indentation experiments and distributions of the linear slope of the indentation curves in the absence and presence of the NP monolayer.

The presence of the silica NP monolayer consistently changes the indentation curves at the water/heptane interface. Data clearly show a softer interface in the presence of the monolayer compared to the free water/heptane interface (Red and blue curves respectively in Fig. 3). Employing the model introduced in reference 34, the linear slope of the force curves is evaluated to be 20±3 mN/m for the free water/heptane interface whereas it is 6±2 mN/m for the interface

covered with a monolayer of 0.05 mM CTAB-decorated NPs. Since the deformability of the liquid interface was found to be comparable to the surface tension at the air/water interface[39], the higher achievable deformation of the interface in the presence of NPs can be interpreted in terms of reduction of the interface free energy[26] facilitated also by interfacially adsorbed CTAB. The combination of topographical images and force curves could therefore be exploited, in the case of multi-component heterogeneous interfaces, to acquire nanoscopically-resolved interface free energy maps.

Moreover, the force curve shows a jump which is interpreted as the maximum local force that a single nanoparticle can withstand before being displaced (red arrow in Fig. 3) which, for the specific systems herein investigated, ranges between 1 and 5 nN. Since the AFM tip size is comparable to the size of a single NP, the discontinuity force value depends on the relative position between them during the indentation process. This kind of force discontinuity events are frequently observed in AFM Force Spectroscopy (AFM-FS) indentation experiments carried out on thin films supported by solid substrates and they are interpreted as rupture events characterizing the mechanical stability of the films[40,41]. In the liquid/liquid interface case, such a rupture event occurs however at large indentation depths of several hundreds of nanometers, since the whole interface is deformed under the pressure of the AFM tip. The Supporting Information reports additional possible events occurring during local indentation experiments performed on fluid interfaces (Fig. S5) including positive jumps in the force. A complete rationale of these events and the proper choice of the experimental setup may allow in future the direct measurement of interfacial forces such as inter-particle interactions, whose quantification and interpretation is currently puzzling the scientific community[42].

In summary, our results open the door to nanoscale resolved imaging in real space in-situ at liquid-liquid interfaces by means of conventional AM-AFM. In this work we have investigated silica NP monolayers adsorbed at a liquid/liquid interface in real space by AM-AFM and reciprocal space

using GISAXS. The correlation between the data sets is high, leading to a powerful new combined approach for studying NP assembly. Our nanoscale AFM imaging resolves single silica nanoparticles and detects defects and isolated 3D structures that might not be captured unambiguously by reciprocal space methods. The approach can also be employed to characterize at the nanoscale in real space thin films such as polymers, emulsifiers or lipids deposited at liquid-liquid interfaces. Finally, the AFM indentation curves permit access to variations of the interfacial stiffness and related interface tension. This will enable the characterization of local changes of the surface tension through 2-dimensional maps which will be particularly interesting for more heterogeneous samples compared to the systems investigated in this work.

Materials and Methods

The 0.1wt% silica NP 1 mM NaCl solutions used in this work were obtained by dilution of Sicastar (Micromod) mother aqueous solutions of charge stabilized bare silica NPs, featuring 10 mg/ml. CTAB (purity $\geq$ 99%), hexane (purity $\geq$ 99%), heptane (purity $\geq$ 99%) and NaCl (purity $\geq$ 99.999%) were all purchased from Sigma Aldrich. Ultrapure deionized water (resistivity 18.2 MΩ·cm, ELGA) was used to prepare the dispersions, which were sonicated for 30 minutes before their characterization.

For GISAXS experiments, the NP dispersion was poured into a polyoxymethylene (POM; Delrin) cell and then gently covered by a macroscopically thick (3-5 mm) layer of hexane. Finally the cell was sealed to prevent hexane evaporation and the NP monolayer was left to stabilize for 30 minutes before starting the measurements.

For AFM experiments, the aqueous dispersion was poured into a home-made cell and then gently covered by hexane. The cell was obtained by drilling a hole into a 100 μm thick mica disk and by gluing it to a second disk. This hole acts as reservoir for the aqueous phase. Its depth was limited to the micron scale (< 100 μm) to minimize the waves originated by deeper water layers. Since this cell was open at the top to allow access for the AFM cantilever, the hexane layer was constantly

refilled to ensure the full coverage of the aqueous phase. Finally, the high evaporation rate of hexane disrupted the execution of AFM measurements, therefore, hexane was replaced by lower vapour-pressure heptane after formation of the NP monolayer. Heptane refilling was then performed every 20 minutes, thus allowing, between each refilling, to acquire several AFM images. AFM images were obtained in Amplitude Modulation mode (AM-AFM). We used an Asylum Research (Oxford Instruments) Cypher AFM. Olympus AC40 cantilevers were employed for imaging. Cantilevers were excited with BluDrive[TM] photothermal excitation. Details on the cantilever excitation are reported in the Supporting Information Section 7 and Fig. S6. The cantilever resonance in heptane was ~ 30 kHz and the free oscillation amplitude was set to 10 nm. Images were acquired at constant amplitude with a set-point ~80% of the free amplitude at a scan rate was in the range 5-10 lines per second. The cantilever stiffness was calibrated employing the thermal method[43]: typically it was close to 150 mN/m. The deflection sensitivity of the photodetector was calibrated acquiring approach-retract curves on a solid surface (mica) in heptane environment during experimental sessions prior to the liquid-liquid interface measurements. For AC40 cantilevers this sensitivity was found to be in the range 10 - 15 nm/V. Indentation measurements were acquired in static mode in a Force Spectroscopy operational scheme (FS-AFM) employing the very same cantilevers used for imaging in AM-AFM. The linear slopes were averaged over 200 indentation curves and plotted in the histograms of Fig. 3. The error reported for the linear slope of the indentation experiments, representing the interface deformability, is propagated from the error resulting from the calibration of the cantilever stiffness through the thermal method (approximately 20%) and from the standard deviation of the linear slope distributions. Supporting Information Fig. S3 and S7 report data from typical experimental sessions which may occur while performing AFM imaging of liquid interfaces. Figure S7 presents an AFM image of the NP system lying on mica due to the disappearance of the water layer after a liquid leakage in the AFM sample holder. Figure S8 suggests that the monolayer is not stable once deposited onto mica since it has the tendency to form aggregates loosing flatness and ordering.

GISAXS measurements were obtained at ID 10 beamline of ESRF. The 22 keV X-ray beam was deflected down to the liquid interface by rotating a Ge deflector crystal around the beam direction and by keeping it at the Ge(111) Bragg reflection. The incident angle was kept at 0.03 degrees (95% of the water/hexane critical angle for total external reflection at 22 keV). The 2D GISAXS patterns were recorded with a Maxipix 5:1detector kept at a distance of 1213.16 mm from the sample center. The resulting 2D scattering patterns (Fig. 2) are presented as a function of q_z and q_y, which are respectively the interface-normal and interface-parallel components of the x-ray momentum transfer.

Supporting Information. Small angle X-ray scattering data of the NP dispersion; high and low resolution AFM images of the monolayers at the liquid-liquid interface; AFM imaging of the drift at the liquid-liquid interface; method for the calculation of the inter-particle distance from the AFM images; AFM and GISAXS data of the CTAB 0.1 mM-decorated silica nanoparticles at the liquid-liquid interface; indentation curves, photothermal excitation of the AFM cantilever; silica nanoparticle monolayer at the mica-heptane interface. This material is available free of charge via the Internet at http://pubs.acs.org.

Corresponding Author

* costa@cbs.cnrs.fr, giolides@unict.it

Author Contributions

The manuscript was written through contributions of all authors. All authors have given approval to the final version of the manuscript. ‡These authors contributed equally.

REFERENCES

[1] Betzig, E.; Patterson, G.H.; Sougrat, R.; Lindwasser, O.W.; Oleynch, S.; Bonifacino, J.S.; Davidson, M.W.; Lippincott-Scwartz, J; Hess, H.F. Science **2006**, 313, 1642-1645

[2] Huang, B. ; Wang, W.; Bates, M.; Zhuang, X. Science **2008**, 319, 810-813.

[3] Jones, S.A.; Shim, S.-H.; He, J.; Zhuang, X. Nat. Meth**. 2011**, 8, 499-505

[4] Garcia, R.; Herruzo, E.T. Nat Nanotech **2012**, 7, 217-226

[5] Schulze, R.; Arras, M.M.L.; Li Destri, G.; Gottschaldt, M.; Bossert, J.; Schubert, U.S.; Marletta, G.; Jandt, K.D.; Keller, T.F. Macromolecules **2012**, 45, 4740-4748

[6] Russo, P.; Acierno, D.; Marletta, G.; Li Destri, G. Eur. Polym. J. **2013**, 49, 3155-3164

[7] Seidler, N.; Lazzerini, G.M.; Li Destri, G.; Marletta, G.; Cacialli, F. J. Mater. Chem. C **2013**, 1, 7748-7757

[8] Li Destri, G.; Miano, F.; Marletta G. Langmuir **2014**, 30, 3345-3353

[9] Ando, T. Nanotechnology **2012**, 23, 062001

[10] Casuso, I.; Khao, J.; Chami, M.; Paul-Gilloteaux, P.; Husain, M.; Duneau, J.P.; Stahlberg, H.; Sturgis, J.N.; Scheuring, S. Nat. Nanotech. **2012**, 7, 525-529.

[11] Ido, S.; Kimiya, H.; Kobayashi, K.; Kominami, H.; Matsuhige, K.; Yamada, H. Nat. Mater. **2014**, 13, 264-270.

[12] Gumí-Audenis, B. ; Carlà, F.; Vitorino, M. V. Panzarella, A.; Porcar, L. Boilot, M.; Guerber, S.; Bernard, P.; Rodrigues, M. S.; Sanz, F. Giannotti, M. I.; Costa, L. J. Synchrotron Radiat **2015**, 22, 1364-1371

[13] Costa, L.; Rodrigues, M.S.; Newman, E.; Zubieta, C.; Chevrier, J.; Comin, F. J. Mol. Recognit. **2013**, 26, 689-693

[14] Uddin, M.H.; Tan, S.Y.; Dagastine, R.R. Langmuir **2011**, 27, 2536-2544

[15] Dubreuil, F.; Daillant, J.; Guenoun, P. Langmuir **2003**, 19, 8409-8415.

[16] Eng, L. M.; Seuret, C.; Looser, H.; Gunter, P. J. Vac. Sci. Technol. B **1996**, 14, 1386-1389.

[17] Boal, A. K.; Ilhan, F.; DeRouchey, J.; Thurn-Albrecht, T., Russell, T.P., Rotello, V.M. Nature **2000**, 404, 746-748.

[18] Lin, Y.; Skaff, H.; Emrick, T.; Dinsmore, A.D.; Russell, T.P. Science **2003**, 299, 226-229.

[19] Schliehe, C.; Juarez, B.H.; Pelletier, M.; Jander, S.; Greshnykh, D.; Nagel, M.; Meyer, A.; Foerster, S.; Kornowski, A.; Klinke, C.; Wller, H. Science **2010**, 329, 550-553.

[20] Glotzer, S.C.; Solomon, M. J. Nature Mater. **2007**, 6, 557-562.

[21] Boneschanscher, M.P.; Evers, W.H.; Geuchies, J.J.; Altantzis, T.; Goris, B.; Rabouw, F.T.; van Rossum, S.A.P.; van der Zant, H.S.J.; Siebbels, L.D.A.; Van Tendeloo, G.; Swart, I.; Hilhorst, J.; Petukhov, A.V.; Bals, S.; Vanmaekelbergh, D. Science **2014**, 344, 1377-1380.

[22] Bera, M. K.; Chan, H.; Moyano, D.F.; Yu, H.; Tatur, S.; Amoanu, D.; Bu, W.; Rotello, V.M.; Meron, M.; Král, P.; Lin, B.; Schlossman, M.L. Nano Lett. **2014**, **14**, 6816-6822.

[23] Sanyal M.K.; Agrawal, V.V.; Bera, M.K.; Kalyanikutty, K.P.; Daillant, J.; Blot, C.; Kubowicz, S.; Konovalov, O.; Rao, C.N.R. J. Phys. Chem. C **2008**, 112, 1739-1743.

[24] Boker, A.; He, J.; Emrick, T.; Russell T.P. Soft Matter **2007**, 3, 1231-1248.

[25] Glokowski, E.; Tangirala R.; He, J.; Russell, T.P.; Emrick, T. Nano Lett. **2007**, 7, 383-393.

[26] Calzolari, D.C.E.; Pontoni, D.; Deutsch, M.; Reichert, H.; Daillant, J. Soft Matter **2012**, 8, 11478-11483.

[27] Maestro, A.; Deshmukh, O. S.; Mugele, F.; Langevin D. Langmuir **2015**, 31, 6289-6297.

[28] Garcia, R. Amplitude Modulation Atomic Force Microscopy. **2010** Wiley-VCH Verlag & Co., Wenheim.

[29] Herruzo, E.T.; Asakawa, H.; Fukuma, T.; Garcia, R. Nanoscale **2013**, 5, 2678-2685

[30] Als-Nielsen, J. ; Jacquemain, D. ; Leveiller, F. ; Lahav, M. ; Leiserowitz, L. Phys. Rep. **1994**, 248, 251-313 (1994).

[31] Ramos, D.; Tamayo, J.; Mertens, J.; Calleja, M. Appl. Phys. Lett. **2006**, 99, 124904.

[32] Garbin, V.; Jenkins, I.; Sinno, T.; Crocker, J.C.; Stebe, K.J.. Phys. Rev. Lett. **2015**, 14, 108301.

[33] Li Destri, G.; Malfatti Gasperini, A.A.; Konovalov, O. Langmuir **2015**, 31, 8856-8864.

[34] Dagastine, R.R.; White, L.R. J. Colloid Interface Sci. **2002**, 247, 310-320.

[35] Dagastine, R.R. ; Manica, R.; Carnie, S.L. ; Chan, D.Y. ; Stevens, G.W.; Griese, F. Science **2006**, 313, 210-213.

[36] Iyer, S.; Gaikwad, R.M.; Subba-Rao, V.; Woodworth, C.D.; Sokolov, I. Nat. Nanotech. **2009**, 4, 389-393.

[37] Stolz, M.; Gottardi, R.; Raiteri, R.; Miot, S.; Martin, I.; Imer, R.; Staufer, U.; Raducanu, A.; Düggelin, M.; Baschong, W.; Daniels, A.U.; Freidrich, N.F.; Aszodi, A.; Aebi, U. Nat. Nanotech. **2009**, 4, 186-192.

[38] Costa, L.; Rodrigues, M.S.; Benseny-Cases, N.; Mayeux, V.; Chevrier, J.; Comin, F. PLOS ONE **2014**, 9, (2014).

[39] Dupré de Baubigny, J.; Benzaquen, M.; Fabié, L.; Delmas, M.; Aimé, J.P.; Legros, M.; Ondarçuhu, T. Langmuir **2015**, 31, 9790-9798.

[40] Gumi-Audenis, B.; Sanz, F.; Giannotti, M. I. Soft Matter **2015**, 11, 5447-5454.

[41] Redondo-Morata, L.; Giannotti, M.I.; Sanz, F. Langmuir **2012**, 28, 12851-12860.

[42] Silvera Batista, C.A.; Larson, R.G.; Kotov, N.A. Science **2015**, 350, 1242477.

[43] Butt, H.J.; Jaschke, M. Nanotech. **1995**, 6, 1-7.